Volume 11
Number 37
7 October 2023
Pages 8825–9038

Journal of Materials Chemistry B

Materials for biology and medicine

rsc.li/materials-b

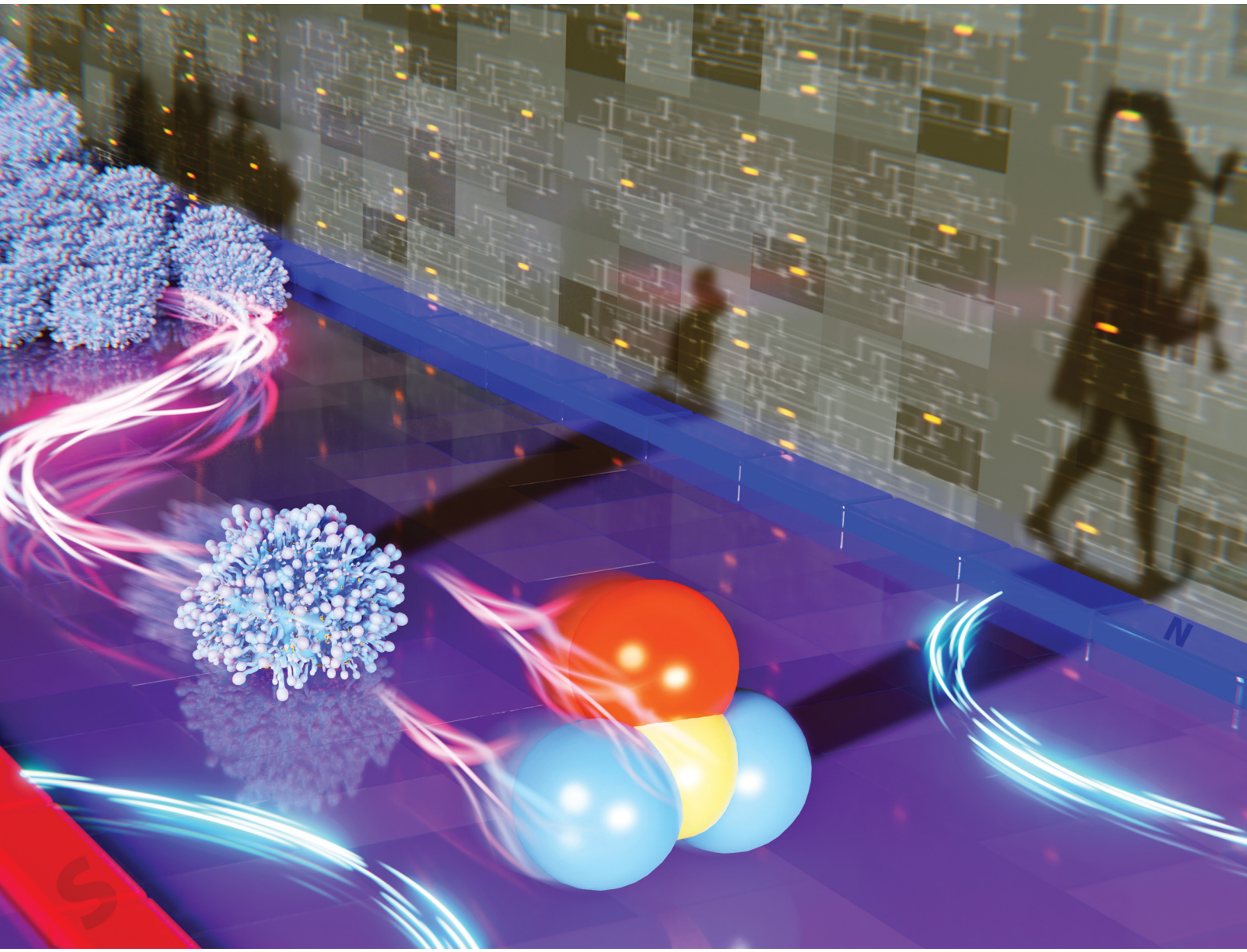

ISSN 2050-750X

ROYAL SOCIETY OF CHEMISTRY

PAPER
Sambeeta Das *et al.*
Fabrication of three-lobed magnetic microrobots for cell transportation

10 YEARS ANNIVERSARY

Journal of Materials Chemistry B

ROYAL SOCIETY OF CHEMISTRY

PAPER

View Article Online
View Journal | View Issue

Cite this: J. Mater. Chem. B, 2023, 11, 8926

Fabrication of three-lobed magnetic microrobots for cell transportation†

Zameer Hussain Shah, Max Sokolich, Sudipta Mallick, David Rivas and Sambeeta Das*

Received 23rd March 2023,
Accepted 6th July 2023

DOI: 10.1039/d3tb00613a

rsc.li/materials-b

Mobile microrobots have the potential to transform medical treatments based on therapeutic delivery. Specifically, microrobots are promising candidates for cell transportation in cell-based therapies. Despite recent progress in cellular manipulation by microrobots, there is a significant need to design and fabricate microrobots to advance the field further. In this work, we present a facile approach to manufacturing three-lobed microrobots by a bench-top procedure. The microrobots are actuated by a harmless magnetic field which makes them biofriendly. Chemically, these microrobots are made of organosilica. The microrobots showed equally good control in both the open-loop and closed-loop settings. The three-lobed microrobots have two modes of motion during the open-loop control experiments. We employed these two modes for single-cell transportation. Our results show that the three-lobed microbots are very promising for cell transportation in a fluid.

Introduction

The untethered microrobots can deliver therapeutics minimally and noninvasively[1] to inaccessible regions of the human body.[2,3] They can potentially revolutionize many applications in biomedicine, such as sensing,[4] drug delivery,[5] regenerative medicine,[6] *etc.* Microrobots are also excellent candidates for cellular applications in regenerative medicine owing to their ability to penetrate the cells rapidly and effective intracellular delivery.[3] Regenerative medicine promises to restore damaged or diseased tissues and organs[7] by cell-based therapy.[8] The cell-based therapies require the transportation of cells to the targeted locations for transplantation.[9] This transportation and delivery need to be precise, and a failed cell delivery could cause a serious immune response.[10] Microrobots are very suitable candidates to perform this crucial step for delivering cells accurately and noninvasively.[11]

Microrobots have been reported to transport cells in recent years. Balasubramanian *et al.*[12] developed microengine rockets carrying antibodies on their surface. The antibodies were sensitive to the antigens expressed by cancer cells that helped binding and subsequent transport of the cells over a preselected path. A similar approach was also reported by Gao *et al.*[13] for the transportation of circulating tumor cells. Likewise, Sanchez *et al.*[14] developed chemically propelled microrobots with magnetic control to selectively, load, transport, and deliver multiple cells to specified locations in a fluid. However, all the above-mentioned studies are based on chemically powered microrobots that require high concentrations of a chemical fuel which is toxic for the living cells.[15] As an alternative, magnetically actuated microbots have also been developed for the biological applications.[16] Over the course of last decade, different research groups have developed magnetically actuated microrobots for cell delivery. However, most of these microrobots were fabricated by direct laser writing or other sophisticated manufacturing technologies[17] that are not accessible to the wider research community.

Colloidal synthesis offers a facile fabrication technique that could be easily scaled up for the commercial scale production.[18] The early research on microrobots greatly benefited from the colloidal synthesis where most of the synthesized microrobots were spherical Janus colloids.[19] The Janus microrobots are very promising for the fundamental research,[20] however, for many practical applications, asymmetric microrobots of non-spherical shape are highly desired.[21] The colloidal synthesis of non-spherical microrobots has been rarely reported since it is highly challenging to synthesize these particles.

In the current work, we report the fabrication of three-lobed microrobots by using a bench-top colloidal synthesis route. The particles were coated with a nickel layer for a sharp magnetic response. We demonstrate that these microrobots could be moved to a desired location by controlling them with a rotating magnetic field. The microrobots were evaluated for their controlled motion in open-loop as well as closed-loop settings. They showed a good control in both conditions. Due to their unique shape, they offer promising cargo carrying opportunities.

Department of Mechanical Engineering, University of Delaware, Newark, DE 19716, USA. E-mail: samdas@udel.edu

† Electronic supplementary information (ESI) available. See DOI: https://doi.org/10.1039/d3tb00613a

We show this by transporting cells from one point to another point on a glass substrate.

Experimental setup

We created rotating homogeneous magnetic fields by using an electromagnetic manipulation system. We designed and optimized the coil system is based on a Helmholtz for mounting on an inverted microscope (Zeiss Axiovert 200 M), as shown in Fig. 1a. There are six rings assembled into three pairs to form the coil system. The coils are formed by wrapping the copper wires onto these rings. We used three different sizes of the rings: small, medium, and large. For a better fitting into the working space, the coil rings were mounted vertically (medium and large) and horizontally (small). The larger and smaller coils were made with a diameter of 106 mm and 36 mm, respectively. The diameter of medium-sized coils was 66 mm. The rings and other components of the magnetic setup (platform and slide arm) were designed in the Solidworks software for 3D printing. The printing was carried out with PLA on an Ender 3 Pro machine. The coils were made by wrapping a 24 AWG copper wire onto the rings by using a standard hand drill. A uniform magnetic field of 2 mT was generated for each of the medium and large ring pairs and 4 mT for the small ring pair when a current of 1 A was applied. A motherboard with electrical connections powered the coils. The motherboard was operated wirelessly by a tablet computer connected to an X-box joystick. The X-box controller was used to control the magnetic field direction for the microrobotic manipulation, providing an easy control over the motion-direction of microrobots. This control apparatus is schematically depicted in Fig. 1b.

After optimizing the magnetic setup for microrobotic manipulation, we employed three-lobed microrobots for cell transportation. Three-lobed microrobots can offer several advantages over commonly employed spherical microrobots for cell transportation. The presence of three lobes provides additional points of contact with the environment, increasing stability and reducing the likelihood of the microrobot rolling or slipping during transportation. This enhanced stability can help ensure the microrobot maintains better control while carrying cells. The three-lobed microrobots were synthesized by a modified procedure developed by Sacanna *et al.*[22] Briefly, commercially available magnetic polystyrene microspheres were utilized as seed particles for the heterogeneous nucleation of a polymerizable oil (3-trimethoxysilyl propyl methacrylate; TPM) onto them. The details of heterogeneous nucleation of TPM can be found elsewhere.[22,23] The seed particles were used without any treatment or washing (Fig. 2). The magnetic colloids tend to aggregate as soon as they meet each other. We employed sonication to ensure that most of the particles are singlets. We found that sonication for 1 minute was enough for the particle concentration in our experiments. A longer sonication period was required for higher concentrations of the seed particles. After sonication, hTPM was quickly injected into the solution. Under the basic conditions, TPM goes into hydrolysis and deprotonation that results in the formation of organosilica.[24] The clear suspension turns into milky-white color within a few minutes of the hTPM injection. This white colour comes from the newly formed organosilica droplets by homogeneous and heterogeneous nucleation (Fig. 2b). It is important to note that the organosilica grows onto solid seed particles when the particle surface chemistry is feasible to form a bond with the silica molecules.[22,25–27] Initially, only small droplets grow heterogeneously onto the seed particles.[23] These smaller droplets grow into bigger lobes as we add more precursor solution to the reaction mixture. Interestingly, we observed some little bulges (Fig. 2c) on the middle part of our seed particles. Such bulges have not been reported by other research groups. We speculate that this could be due to a bigger seed particle in our experiments. These bulges could be small organosilica droplets that may come from secondary nucleation. Moreover, our final product is always a mixture of particles with different number of lobes. The number of particles with the same number of lobes is highly influenced by the quality of the seed particles. A highly monodispersed seed particle suspension results in a higher fraction of particles with same number of lobes.[22]

Results and discussion

The magnetic properties of the three-lobed colloids were examined utilizing a vibrating sample magnetometer (VSM). A powdered sample was used by drying the colloidal particles suspension. The

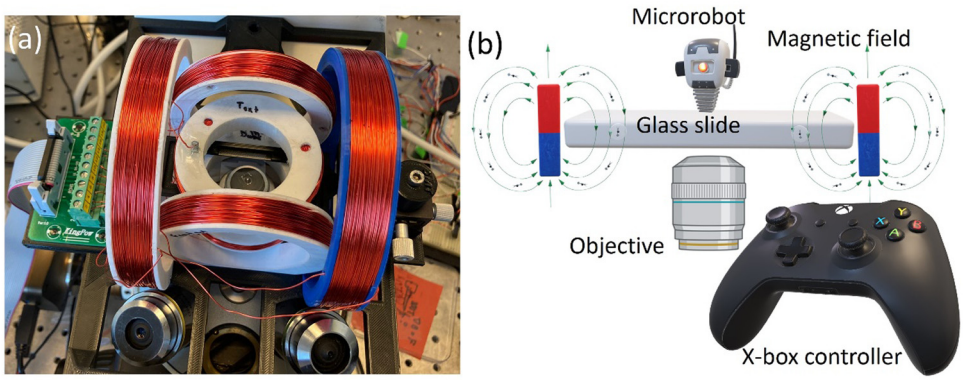

Fig. 1 Magnetic setup for the microrobot control. (a) Helmholtz coils mounted on an inverted microscope and (b) a schematic of microrobotic control employed in this study.

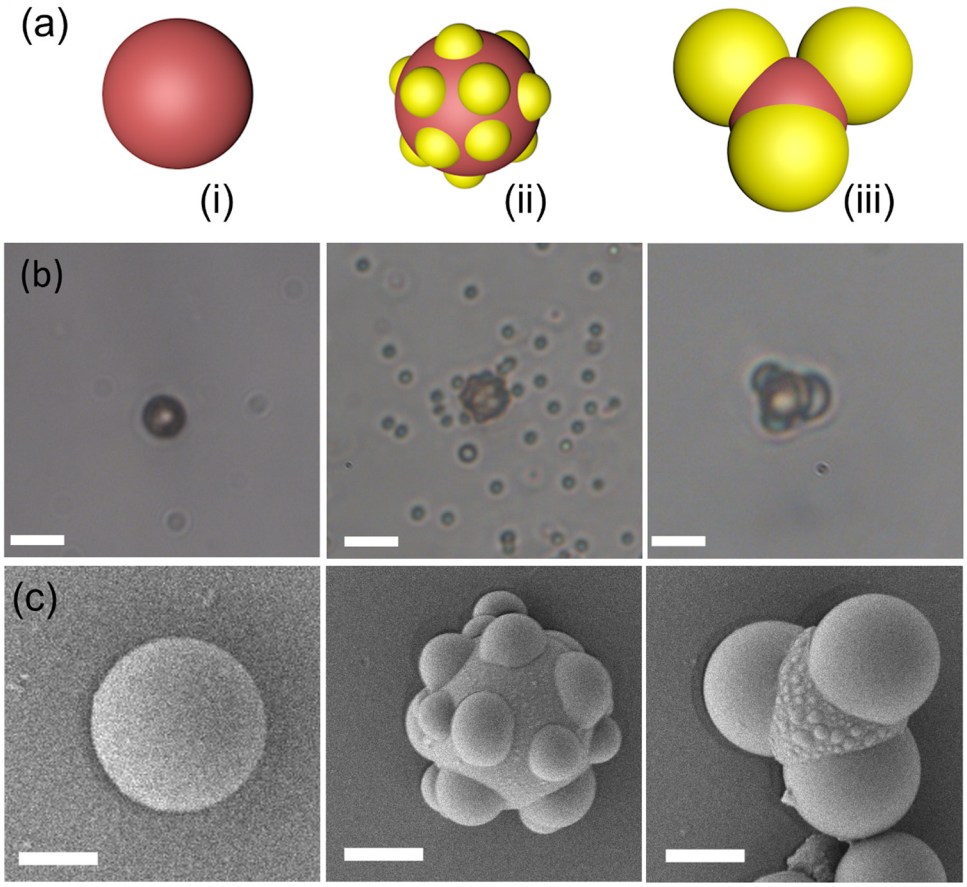

Fig. 2 Synthesis of three-lobed microrobots. (a) Scheme of synthesis (i) magnetic seed particles, (ii) heterogeneous nucleation of oil on the seeds, (iii) growth of droplets to achieve three lobes. (b) and (c) are corresponding respective optical and SEM images captured at different synthesis stages. Scale bars in (b) are 5 μm and in (c) are 2 μm.

VSM analysis revealed a ferromagnetic behavior exhibited by our particles, as demonstrated by the magnetic hysteresis. The coercivity of the particles was approximately 38 Oe, while saturation was achieved at around 2500 Oe. For further reference, the hysteresis loop is provided in Fig. S1 (ESI†).

When a microparticle with an embedded magnetic component is placed in a magnetic field, it experiences a magnetic force $\vec{F}$ given by:

$$\vec{F} = (\vec{m}\cdot\nabla)\vec{B} \quad (1)$$

Where $\vec{B}$ is the magnetic field and $\vec{m}$ is the magnetization or the magnetic moment of the particle. The particle also experiences a magnetic torque $\vec{\tau}$ which can be predicted from the following equation:

$$\vec{\tau} = \vec{m} \times \vec{B} \quad (2)$$

When the magnetic field is turned on, the magnetic moment of the particles aligns itself with the external magnetic field. By changing the direction of the applied magnetic field, the magnetic moment alignment also changes which offers a fundamental tool to control motion at the nanoscale. Eqn (2) implies that by rotating the applied magnetic field in a certain direction by a certain angle will rotate a magnetized particle until magnetic moment is aligned with new direction of the magnetic field.[28]

We utilized a rotating magnetic field to actuate the three-lobed microrobots. Under no magnetic field, these microrobots showed no motion. When the magnetic field is turned on, the microrobots align themselves to the applied magnetic field. Next, by changing the direction of the magnetic field by using the X-box controller, we moved the microrobots in the desired directions. This rolling motion of the three-lobed microrobots is depicted schematically in Fig. 3. It is worth mentioning that the seed particles used for the fabrication of these microrobots are magnetic which makes these microrobots responsive to the magnetic field without any metal coating. However, we found that response was much weaker for the uncoated particles (Video S1, ESI†). It could be because of the increase in the weight of the microrobots due to three big lobes. On the other hand, the nickel-coated particles showed a sharp response to the rotating magnetic field (Fig. 4 and Video S2, ESI†), therefore, we performed all experiments on the nickel-coated microrobots.

The three-lobed microrobots showed no motion in the absence of a magnetic field. As soon as the magnetic field was turned on, the magnetic moment of the microrobots aligned itself to the

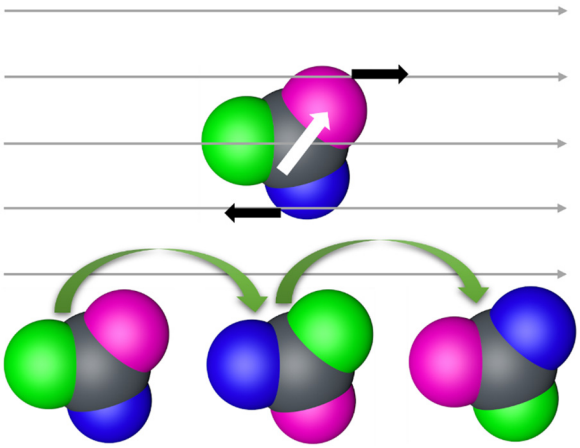

Fig. 3 Schematic of rolling motion of three-lobed microrobots in a rotating magnetic field. White arrow shows the magnetic moment of the microrobots.

magnetic field, as can be seen in Video S2 (ESI†) and Fig. 4 at 1 s. The magnetic response of the microrobots was monitored and recorded by the camera attached to the microscope. Next, the microrobots were moved toward the lower right corner of the screen, as shown at 7 s in Fig. 4. We applied a frequency of 2 Hz to perform all the motion experiments of theses microrobots. Then we moved the particle toward the bottom and upper left corner

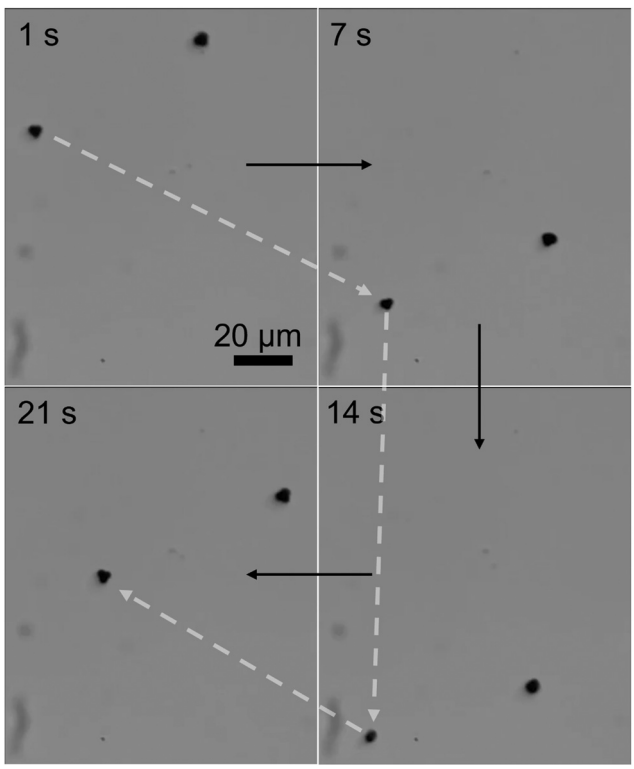

Fig. 4 Motion of three-lobed microrobots in a rotating magnetic field: time-lapse images of translational motion. Two microrobots are shown moving in response to the magnetic field. The motion of one microrobot is highlighted by dashed white arrows.

(Fig. 4, 14 s and 21 s, respectively). Moreover, the microrobots also showed a rotational motion which is achieved just by changing the angle of the applied magnetic field. This rotational motion is shown in Fig. 5 and Video S3 (ESI†).

The microrobotic motion controlled by hand-held devices does not offer a stable and precise motion required for practical applications. Therefore, it is highly desired to control the microrobotic motion by using a closed-loop approach. To test the performance of three-lobed microrobots in closed-loop settings, we applied a closed-loop protocol to these microrobots. This closed-loop protocol is recently developed by Sokolich *et al.*[29] and its details can be found elsewhere. As can be seen in Fig. 6 and Video S4 (ESI†) these microrobots showed very good response to the applied closed-loop instructions. The microrobots reached to the given destination without deviating from its path and automatically stopped after arriving at the desired location.

Next, we employed the three-lobed microrobots for cell transportation. It is interesting to note that we did not apply any sophisticated chemistry on the microrobot surface for the cell–microrobot interaction. Instead, we anticipated that the unique shape of our microrobots will offer enough opportunity for them to physically interact with the Human embryonic kidney (HEK cells). Indeed, we found it to be true. During their linear motion, the three-lobed particles appear to be standing. This posture offers a better contact between the microrobot and any other micron sized object. Interestingly, when the microrobots were in contact with the HEK cells, they did not show a similar rolling motion as observed in prior experiments. Instead, the microrobots appear to be wobbling *via* the rotational magnetic field. This wobbling motion of the microrobots was sufficient to transport the cells from one point to another point, as shown in Fig. 7 and Video S5 (ESI†). Since the cell has

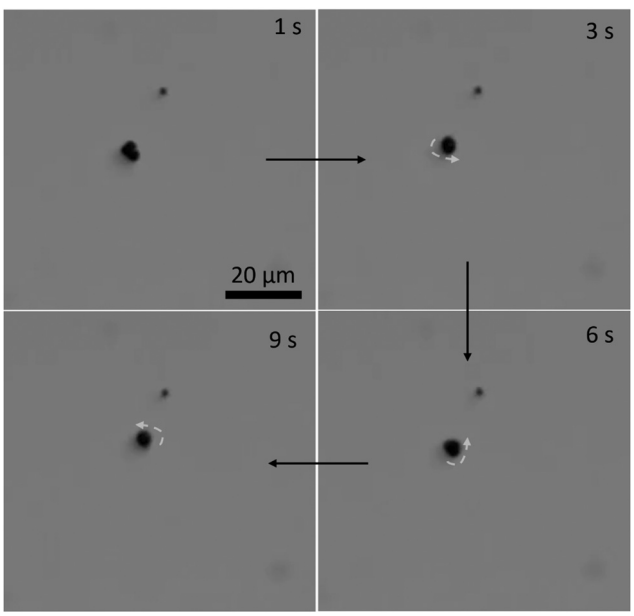

Fig. 5 Rotational motion of the three-lobed microrobot: time-lapse images of a microrobot at different stages of rotational motion.

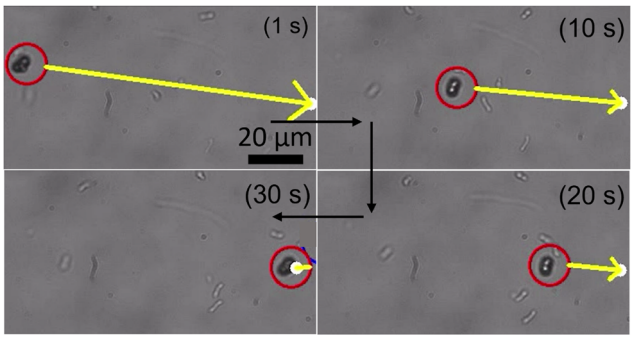

Fig. 6 Closed-loop control of the three-lobed microrobots. The yellow arrow is pointing in the direction of the applied magnetic field.

a spherical shape, it was hard to keep the contact between the cell and the microrobot for a longer period. Therefore, during the motion the cell would occasionally get detached from the microrobot. However, it was not difficult to bring back the microrobot to the cell to carry its motion in a particular direction.

As we presented in Fig. 5, the three-lobed microrobots have two modes of motion. The translational motion offered a contact-based transportation of the cells. On the other hand, we also studied the influence of rotational motion of the microrobots on neighbouring cells. As it can be predicted that a rotational motion of a microrobot in a fluid will generate a flow. The strength of this flow will determine its influence on the passive particles in the surrounding environment. We show the effect of rotational motion of a microrobot on a neighbouring cell in Fig. 8 and Video S6 (ESI†). As soon as the rotational motion of the microrobot started (at 1 s) the cell responded to the generated flow and started to move clockwise on a circular trajectory. This offers a contactless transportation of a cell in confined space. We envision that a combination of translational and rotational modes of cell transport could be more beneficial for a better control in transportation.

It is important to know the cytotoxicity of microrobots for practical applications. Generally, Ni coated microrobots are coated with a thin layer of Ti to avoid any toxic effects from Ni.[30,31] In our study, we used very dilute suspension of the microrobots since we were aiming for single cell transportation, therefore, we studied the cytotoxicity of our microrobots without coating them with an additional Ti layer. During these experiments, we found that the cell morphology and growth pattern of Chinese hamster Ovarian (CHO) cells was intact after 24 h of treatment with the three-lobed microrobots (Fig. 9a and b). Interestingly, cells were seen attached to the microrobots owing to the non-toxic silica surface of the microrobots (Fig. 9b). Moreover, cells were stained with trypan blue to assess cell viability after microrobot treatment. Considering the floating nature of dead cells, supernatant was collected and stained with trypan blue. Cell death was comparable with control group and there were no dead cells found after 24 h with the microrobots attached to them (Fig. S2, ESI†). Moreover, no significant toxic effect was observed after 48 h. Effect of actuation on CHO cells was also assessed. Cell proliferation was unaffected 24 h after

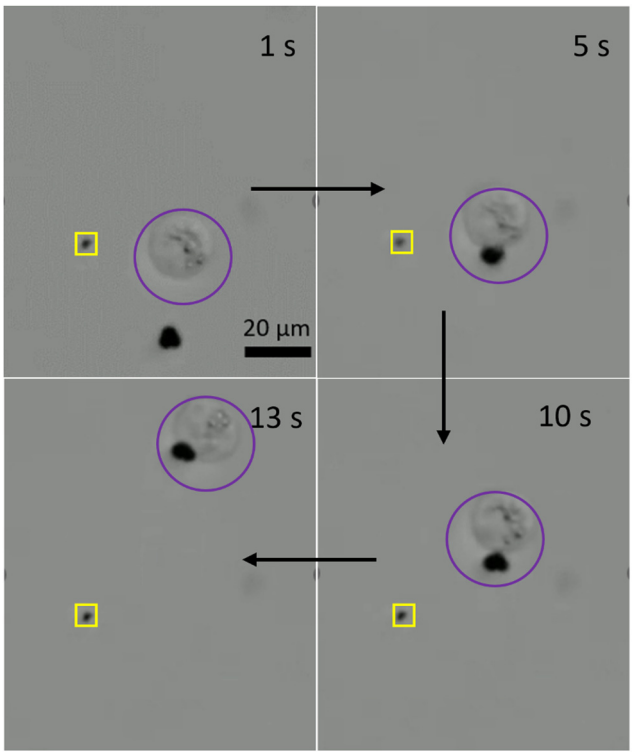

Fig. 7 Cell transportation by three-lobed microrobots. Time-lapse optical images of a microrobot transporting a cell. Yellow square is the reference point to mark a change in the position of cell being transported.

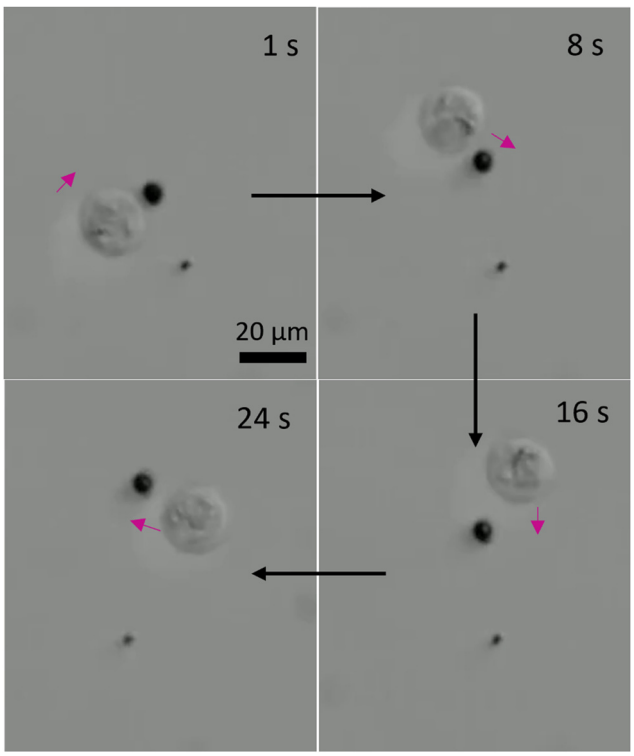

Fig. 8 Contactless transportation of a cell by a rotating microrobot.

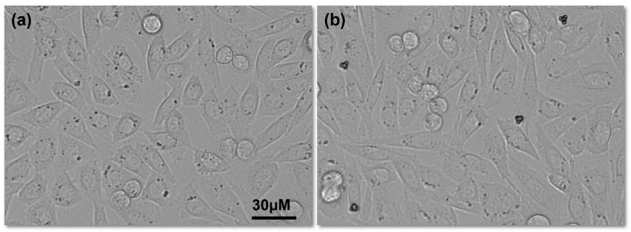

Fig. 9 Cell morphology and growth after 24 h: (a) cells without any microrobots and (b) cells with three-lobed microrobots.

actuation and the characteristic spindle morphology of CHO cell was intact (Fig. S3, ESI†). Therefore, these microrobots are promising to explore for further biomedical applications.

Conclusions

In summary, we have fabricated three-lobed microrobots that are actuated by a magnetic field. The synthesis was based on the heterogeneous nucleation and subsequent polymerization of organosilica precursor on the solid seed particles. The microrobots were controlled by open-loop as well as closed-loop programs. In the open loop experiments, the microrobots demonstrated translational and rotational modes of motion. The three-lobed microrobots were tested for cell transportation and it was found that these are excellent candidates for single cell transportation in a fluid.

Materials and methods

Chemicals

Magnetic polystyrene particles (MPS), Nile red (4.35 μm, 1.0% w/v) were provided by Spherotech. Ammonia solution (25% wt) was purchased from Acros Organics. 2,2′-Azobis (2-methylpropionitrile) (AIBN, 98%) and 3-trimethoxysilyl propyl methacrylate (TPM) were obtained from Sigma Aldrich. Deionized (DI) water (Millipore, 18.2 mΩ) was used in all experiments.

Synthesis of three-lobed particles

60 ml DI water was taken in a 100 ml glass bottle and stirred magnetically at 500 rpm. Then 6 ml of TPM was added to it. The mixture was stirred at room temperature for about 5 h, after which it was a clear solution of hydrolyzed TPM (hTPM). Next, 10 ml of DI water was taken in a 30 ml glass vial, and 5 μl of the ammonia solution was added to it. The seed particles were added to this solution (0.1 ml), and the particle suspension was sonicated for 1 min. Then, 4.0 ml of hTPM was injected into this solution and gently hand-mixed. The mixture was left undisturbed on a bench for 20 minutes. Next, 2.0 ml hTPM was added to the mixture after every 20 minutes until the desired morphology was achieved. Finally, 5 mg AIBN was added, and the reaction mixture was placed in a preheated oven at 80 °C for 3 h. The particles were washed with DI water and purified by repeated washing and centrifugation cycles several times.

Metal deposition on the three-lobed particles

The purified particles were dispersed on a glass substrate, and water was allowed to evaporate. The dried particles were coated with a 50 nm Ni layer using a dual e-beam deposition machine. The particles were recovered by mopping a wet lens-cleaning paper onto the glass slide and its subsequent suspension in 0.5 ml DI water in a 1.5 ml plastic vial. The transfer of particles from the paper surface into the water was achieved by vortex mixing for a few seconds.

Magnetic characterization of microrobots

In this study, the magnetic saturation of three-lobed microrobots was measured using a vibrating sample magnetometer (VSM). The microrobot sample was securely positioned within a sample holder integrated into the optical magnetomechanical device (OMMD). To initiate the measurements, the power supply was activated, and the voltage was set to 3 V.

Cytotoxicity of microrobots

Cytocompatibility of microrobots was assessed in Chinese Hamster Ovarian (CHO) cells. Cells were cultured in Dulbecco's Modified Essential Medium/Nutrient Mixture F-12 (DMEM/F-12, Gibco, BenchStable, USA) media with 5% CO_2, and maintained at 37 °C in an incubator. All experiments were performed after second passage, and by eighth passage. Cells were incubated with different microrobots for 24 h. Then, cells were imaged under the microscope (Zeiss Axiovert 200). Cytotoxicity was assessed by Trypan blue staining. All floating cells in the supernatant were collected and stained with trypan blue after 24 h and 48 h treatment. Effect of actuation was also assessed on CHO cells. Images of cells after actuation were taken immediately after actuation and 24 h post-actuation.

Conflicts of interest

There are no conflicts to declare.

Acknowledgements

This work is supported by an Institutional Development Award (IDeA) from the NIGMS of the National Institutes of Health under grant number U54-GM104941, from the NIGMS of the National Institute of Health under grant number 1R35GM147451, from the National Science Foundation under grant number 2020973 and under grant number 2218980. We are very grateful to Professor John Q. Xiao and Subhash Bhat from the Electromagnetic Materials Research Laboratory of the University of Delaware for performing the magnetic characterization of our particles.

References

1 B. J. Nelson, I. K. Kaliakatsos and J. J. Abbott, *Annu. Rev. Biomed. Eng.*, 2010, **12**, 55–85.
2 J. Choi, J. Hwang, J.-Y. Kim and H. Choi, *Adv. Healthcare Mater.*, 2021, **10**, 2001596.

3 P. L. Venugopalan, B. Esteban-Fernández de Ávila, M. Pal, A. Ghosh and J. Wang, *ACS Nano*, 2020, **14**, 9423–9439.
4 M. Sitti, H. Ceylan, W. Hu, J. Giltinan, M. Turan, S. Yim and E. Diller, *Proc. IEEE*, 2015, **103**, 205–224.
5 X. Song, R. Sun, R. Wang, K. Zhou, R. Xie, J. Lin, D. Georgiev, A.-A. Paraschiv, R. Zhao and M. M. Stevens, *Adv. Mater.*, 2022, **34**, 2204791.
6 J. Li, X. Li, T. Luo, R. Wang, C. Liu, S. Chen, D. Li, J. Yue, S.-H. Cheng and D. Sun, *Sci. Rob.*, 2018, **3**, eaat8829.
7 A. S. Mao and D. J. Mooney, *Proc. Natl. Acad. Sci. U. S. A.*, 2015, **112**, 14452–14459.
8 D. M. Hoang, P. T. Pham, T. Q. Bach, A. T. L. Ngo, Q. T. Nguyen, T. T. K. Phan, G. H. Nguyen, P. T. T. Le, V. T. Hoang, N. R. Forsyth, M. Heke and L. T. Nguyen, *Signal Transduction Targeted Ther.*, 2022, **7**, 272.
9 N. H. Yu, S. Y. Chun, Y. S. Ha, H. T. Kim, D. H. Kim, J. Kim, J. W. Chung, J. N. Lee, P. H. Song, E. S. Yoo, B. S. Kim and T. G. Kwon, *Tissue Eng. Regener. Med.*, 2018, **15**, 639–647.
10 P. A. Beachy, S. S. Karhadkar and D. M. Berman, *Nature*, 2004, **432**, 324–331.
11 W. Chen, H. Zhou, B. Zhang, Q. Cao, B. Wang and X. Ma, *Adv. Funct. Mater.*, 2022, **32**, 2110625.
12 S. Balasubramanian, D. Kagan, C.-M. Jack Hu, S. Campuzano, M. J. Lobo-Castañon, N. Lim, D. Y. Kang, M. Zimmerman, L. Zhang and J. Wang, *Angew. Chem., Int. Ed.*, 2011, **50**, 4161–4164.
13 W. Gao and O. C. Farokhzad, *Angew. Chem., Int. Ed.*, 2011, **50**, 7220–7221.
14 S. Sanchez, A. A. Solovev, S. Schulze and O. G. Schmidt, *Chem. Commun.*, 2011, **47**, 698–700.
15 S. Sánchez, L. Soler and J. Katuri, *Angew. Chem., Int. Ed.*, 2015, **54**, 1414–1444.
16 M. Sitti and D. S. Wiersma, *Adv. Mater.*, 2020, **32**, 1906766.
17 J. Li and M. Pumera, *Chem. Soc. Rev.*, 2021, **50**, 2794–2838.
18 Y. Pu, F. Cai, D. Wang, J.-X. Wang and J.-F. Chen, *Ind. Eng. Chem. Res.*, 2018, **57**, 1790–1802.
19 Q. Chen, J. Yan, J. Zhang, S. C. Bae and S. Granick, *Langmuir*, 2012, **28**, 13555–13561.
20 B. Jurado-Sánchez, M. Pacheco, R. Maria-Hormigos and A. Escarpa, *Appl. Mater. Today*, 2017, **9**, 407–418.
21 A. Sahari, D. Headen and B. Behkam, 2012 Annual International Conference of the IEEE Engineering in Medicine and Biology Society, 2012.
22 S. Sacanna, M. Korpics, K. Rodriguez, L. Colón-Meléndez, S.-H. Kim, D. J. Pine and G.-R. Yi, *Nat. Commun.*, 2013, **4**, 1688.
23 Y. Liu, K. V. Edmond, A. Curran, C. Bryant, B. Peng, D. G. A. L. Aarts, S. Sacanna and R. P. A. Dullens, *Adv. Mater.*, 2016, **28**, 8001–8006.
24 C. van der Wel, R. K. Bhan, R. W. Verweij, H. C. Frijters, Z. Gong, A. D. Hollingsworth, S. Sacanna and D. J. Kraft, *Langmuir*, 2017, **33**, 8174–8180.
25 M. Youssef, T. Hueckel, G.-R. Yi and S. Sacanna, *Nat. Commun.*, 2016, **7**, 12216.
26 Z. H. Shah, S. Wang, L. Xian, X. Zhou, Y. Chen, G. Lin and Y. Gao, *Chem. Commun.*, 2020, **56**, 15301–15304.
27 W. Xie, C. Zhou, X. Zhang, S. Du, W. Wang, H. Wang and Z. Zhang, *ChemNanoMat*, 2020, **6**, 1749–1753.
28 M. T. Hou, H.-M. Shen, G.-L. Jiang, C.-N. Lu, I.-J. Hsu and J. A. Yeh, *Appl. Phys. Lett.*, 2010, **96**, 024102.
29 M. Sokolich, D. Rivas, Z. H. Shah and S. Das, *arXiv*, 2022, preprint, arXiv:2210.11460, DOI: **10.48550/arXiv.2210.11460**.
30 S. Kim, F. Qiu, S. Kim, A. Ghanbari, C. Moon, L. Zhang, B. J. Nelson and H. Choi, *Adv. Mater.*, 2013, **25**, 5863–5868.
31 S. Tottori, L. Zhang, F. Qiu, K. K. Krawczyk, A. Franco-Obregón and B. J. Nelson, *Adv. Mater.*, 2012, **24**, 811–816.

